# Location of KCNE1 relative to KCNQ1 in the $I_{KS}$ potassium channel by disulfide cross-linking of substituted cysteines

David Y. Chung[a], Priscilla J. Chan[a], John R. Bankston[a], Lin Yang[b], Guoxia Liu[b], Steven O. Marx[a,b], Arthur Karlin[c,1], and Robert S. Kass[a,1]

Departments of [a]Pharmacology; [b]Medicine, Biochemistry and Molecular Biophysics, Physiology and Cellular Biophysics, and Neurology; and [c]Center for Molecular Recognition, College of Physicians and Surgeons, Columbia University, New York, NY 10032

Contributed by Arthur Karlin, November 24, 2008 (sent for review June 6, 2008)

**The cardiac-delayed rectifier $K^+$ current ($I_{KS}$) is carried by a complex of KCNQ1 (Q1) subunits, containing the voltage-sensor domains and the pore, and auxiliary KCNE1 (E1) subunits, required for the characteristic $I_{KS}$ voltage dependence and kinetics. To locate the transmembrane helix of E1 (E1-TM) relative to the Q1 TM helices (S1–S6), we mutated, one at a time, the first four residues flanking the extracellular ends of S1–S6 and E1-TM to Cys, coexpressed all combinations of Q1 and E1 Cys-substituted mutants in CHO cells, and determined the extents of spontaneous disulfide-bond formation. Cys-flanking E1-TM readily formed disulfides with Cys-flanking S1 and S6, much less so with the S3-S4 linker, and not at all with S2 or S5. These results imply that the extracellular flank of the E1-TM is located between S1 and S6 on different subunits of Q1. The salient functional effects of selected cross-links were as follows. A disulfide from E1 K41C to S1 I145C strongly slowed deactivation, and one from E1 L42C to S6 V324C eliminated deactivation. Given that E1-TM is between S1 and S6 and that K41C and L42C are likely to point approximately oppositely, these two cross-links are likely to favor similar axial rotations of E1-TM. In the opposite orientation, a disulfide from E1 K41C to S6 V324C slightly slowed activation, and one from E1 L42C to S1 I145C slightly speeded deactivation. Thus, the first E1 orientation strongly favors the open state, while the approximately opposite orientation favors the closed state.**

arrhythmias | cardiac repolarization | electrophysiology | atrial fibrillation | S1

The slow, outwardly rectifying $K^+$ current ($I_{KS}$) is one of two delayed rectifier $K^+$ currents critical for repolarization of the heart, particularly during sympathetic nervous system stimulation (1, 2). The $I_{KS}$ channel is composed of four pore-forming KCNQ1 (Q1) subunits and two auxiliary KCNE1 (E1) subunits (3–5). Several human mutations in Q1 and E1 cause variants of long QT syndrome (6), short QT syndrome (7), or atrial fibrillation (8, 9).

Although a tetramer of Q1 subunits alone forms a voltage-gated channel, only Q1 and E1 together form a channel with the slow activation and deactivation kinetics and the minimal inactivation characteristics of $I_{KS}$ (10, 11). Furthermore, E1 is necessary for sympathetic modulation of $I_{KS}$ (12). How E1 exerts its effect on Q1 is not yet fully understood.

There have been a number of conclusions about Q1-E1 interactions in the $I_{KS}$ channel, not all of which are compatible. There is evidence for (13) and against (14, 15) the contribution of E1 to the pore wall and its accessibility from the pore. There is also evidence that E1 interacts with the pore domain, although not necessarily exposed in the pore (16, 17), that the E1 TM helix (E1-TM) interacts directly with Q1 S4 helix (18), that E1 modulates Q1 through its C terminus (19–21), and that E1 interacts with the cytoplasmic Q1 S4-S5 linker (22).

More recently, a site of possible Q1-E1 interaction was suggested by the association of mutations in Q1 S1 with congenital atrial fibrillation (8, 9). Either of these S1 mutants, S140G and V141M, when expressed heterologously, appears constitutively open, but only in the presence of E1 (8, 9). It has been shown that E1 is close enough to S1 for spontaneous cross-linking to occur between cysteines substituted in the two regions (23).

With the goal of further defining the structural interactions between Q1 and E1, we determined the proximities of the extracellular end of the E1-TM to the extracellular ends of the Q1 TM helices, S1 through S6, by disulfide cross-linking between cysteines (Cys) substituted for native residues. Disulfide cross-linking has been widely used to determine quaternary structures of proteins and to determine regions that move during changes in functional states (24). Using our variation of this approach (25, 26), we substituted Cys, one at a time, in the first four positions just flanking the extracellular ends of Q1 S1–S6 and just flanking the extracellular end of the E1-TM. We expressed 80 distinct pairs of Cys-substituted Q1 and Cys-substituted E1 in CHO cells and determined the extents of spontaneous disulfide bond formation between Q1 and E1 in channels expressed on the cell surface. Taken together with the high-resolution structure of $K_v1.2$ (27) and a structural model of Q1 (28), our results indicate that the extracellular end of the E1-TM lies between S1 and S6 of two Q1 subunits.

## Results

**Cys Substitutions in Q1 and E1.** The membrane-embedded portions of the TM helices of Q1 (Fig. 1*A* and *C*) and E1 (Fig. 1 *B* and *D*) were predicted by the PHDhtm algorithm (29) and by alignment with the homologous S1–S6 helices of $K_vAP$ (30) and $K_v1.2$ (27). We selected the first four residues just flanking the extracellular ends of the Q1 and E1 TM helices to mutate individually to Cys (Fig. 1). Because these cysteines are exposed to water, they can deprotonate to the reactive thiolate form. They are also constrained approximately to the same plane relative to the membrane, where, depending on their proximity, they are subject to catalytic or spontaneous oxidation in the endoplasmic reticulum or on the cell surface (25).

We generated a total of 20 Cys-substituted mutants of Q1 and 4 Cys-substituted mutants of E1. In Q1, the single-Cys mutations were made in a pseudo-wild-type (pWT) construct in which

Author contributions: D.Y.C., S.O.M., A.K., and R.S.K. designed research; D.Y.C., P.J.C., J.R.B., L.Y., and G.L. performed research; D.Y.C., A.K., and R.S.K. contributed new reagents/analytic tools; D.Y.C., S.O.M., A.K., and R.S.K. analyzed data; and D.Y.C., S.O.M., A.K., and R.S.K. wrote the paper.

The authors declare no conflict of interest.

[1]To whom correspondence may be addressed at: Department of Pharmacology, College of Physicians and Surgeons of Columbia University, 630 West 168th Street, New York, NY 10032. E-mail: ak12@columbia.edu or rsk20@columbia.edu.

This article contains supporting information online at www.pnas.org/cgi/content/full/0811897106/DCSupplemental.

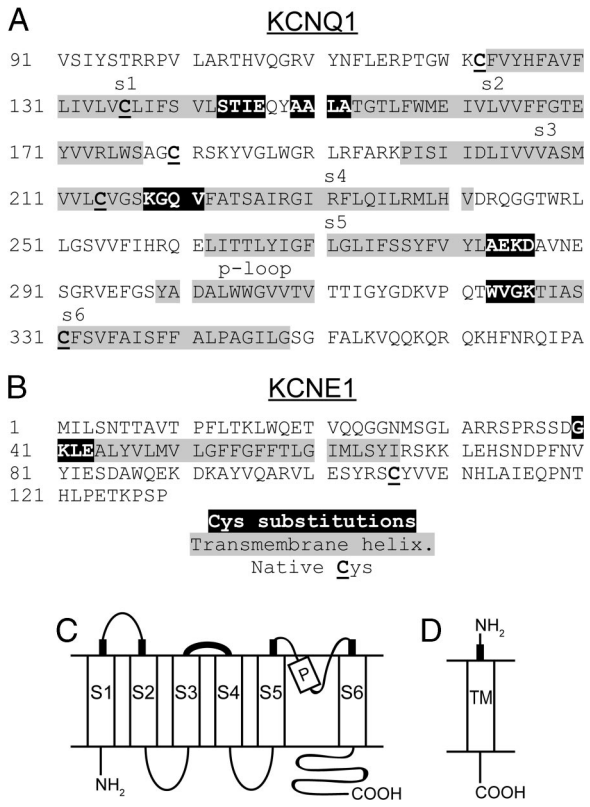


**Fig. 1.** Sequences and membrane topologies of KCNQ1 and KCNE1. (*A*) Q1 sequence. (*B*) E1 sequence. In both sequences, residues (in reverse contrast) flanking the extracellular ends of the transmembrane helices (in gray) were substituted by Cys in pseudowild-type (pWT) Q1. In both subunits, native Cys are underlined and in bold. In pWT Q1, Cys-214 and Cys-331 were mutated to Ala. The membrane topologies of (*C*) Q1 and (*D*) E1 are shown with the extracellular flanking regions, in which cysteines were substituted, indicated by thickened lines.

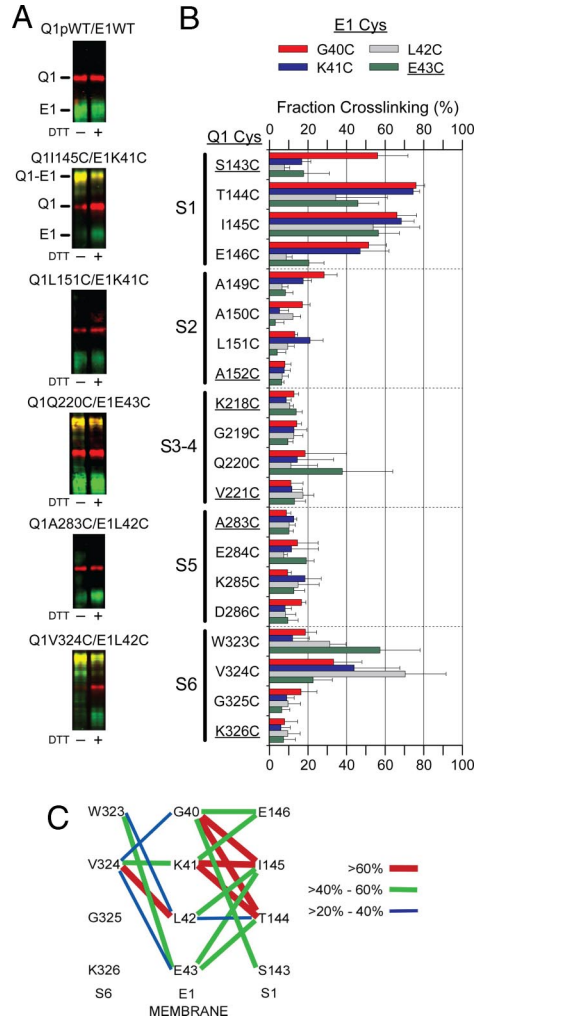


**Fig. 2.** Extent of spontaneous disulfide bond formation between substituted Cys in KCNQ1 and KCNE1. (*A*) Sample immunoblots are shown for pWT Q1 and WT E1 and for the indicated pairs of Cys mutants of Q1 and E1. Q1 is represented as a red signal and E1 as a green signal. The merged red and green in the cross-linked Q1-E1 band is yellow. The samples in the right lanes were reduced with DTT in sample buffer. Slower moving bands are not shown (see Fig. S4). (*B*) The extent of spontaneous cross-linking of each of the 20 flanking Cys in Q1 paired with each of four flanking Cys in E1 is plotted with standard errors. Each Q1 mutant is identified along the vertical axis, and the bar for each E1 mutant is color-coded as in the legend (red G40C, blue K41C, gray L42C, and green E43C). The substituted Cys closest to the transmembrane helices are underlined. (*C*) The extents of cross-linking from E1 to S1 and to S6 are represented by lines connecting the cross-linked positions. See *Legend*.

Cys-214 and Cys-331, two of the three native Cys in the transmembrane domain of Q1, were mutated to Ala (Fig. 1*A*). As detected by western blotting, pWT Q1 expressed in CHO cells as well as WT (Fig. 2). Also, cells expressing pWT Q1 and WT Q1 yielded similar current densities (see Fig. S1). Because mutation to Ala (15), Val, or Ser of the third native Cys in Q1, Cys-136, significantly altered channel function (data not shown), it was not altered in pWT Q1. There was no cross-linking of pWT Q1 to coexpressed WT E1 (Fig. 2*A*). In addition, there was no cross-linking of any Q1 Cys mutant to WT E1 and no cross-linking of any E1 Cys mutant to pWT Q1 (data not shown).

**Cross-Linking.** All 80 possible pairs of Q1 and FLAG-tagged E1 Cys mutants were coexpressed in CHO cells. These cells were reacted with the impermeant sulfoNHS-LC-biotin to label proteins expressed on the cell surface, the reaction was quenched, and the cells were washed and lysed. Biotinylated Q1 and E1 were captured and released from neutravidin beads, electrophoresed in SDS, transferred to nitrocellulose, and detected with anti-Q1 and anti-FLAG antibodies (Fig. 2*A*). The apparent molecular weight of Q1 was ≈70 kDa and that of E1 was 40 kDa, characteristic of maturely glycosylated and surface expressed E1 (31). The cross-linked heterodimer of Q1 and E1 was detected as a band of apparent molecular weight of 110 kDa (Fig. 2*A*). The extent of cross-linking in each lane was calculated as described in the Materials and Methods.

All four Cys flanking S1 were cross-linked >50% to E1 G40C (Fig. 2 *B* and *C*). This is consistent with relatively free rotation of the S1 flank and flexibility of the E1 flank. Although both residues next to the membrane, S1 S143C and E1 E43C, readily formed cross-links with other E1 and Q1 Cys, respectively, they did not readily cross-link to each other (Fig. 2 *B* and *C*). Nevertheless, there was extensive cross-linking of most other pairs of S1 and E1 Cys. The most extensive cross-links were between the E1 residues furthest from the membrane, G40C and K41C, and the two residues, T144C and I145C in the middle of the S1 flank (Fig. 2 *B* and *C*).

On the other side of E1, the two E1 Cys closest to the membrane, L42C and E43C, formed cross-links most readily with the two residues in the S6 flank, W323C and V324C, furthest from the membrane (Fig. 2 *B* and *C*). This is consistent again with flexibility of the E1-TM flank; however, unlike the S1 flank, S6 and its flank are likely to have a relatively fixed axial orientation.

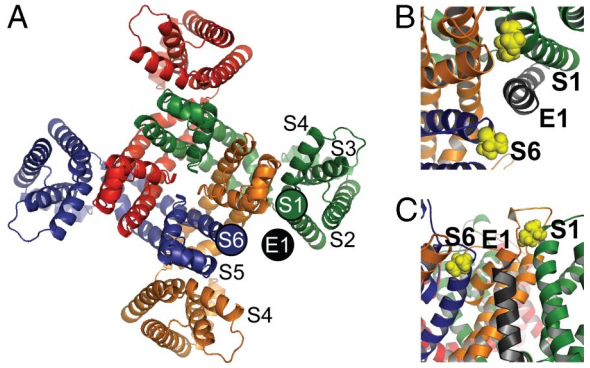


**Fig. 3.** Placement of E1 within the $I_{Ks}$ channel complex. (*A*) Extracellular view of a tetramer of Q1 from Smith *et al.* with superimposed E1-TM. The extracellular ends of the S1 and S6 helices of two different Q1 subunits are indicated by filled circles, color-coded like the underlying model. Our proposed location of the extracellular end of one E1-TM is shown as a black circle. (*B*) Extracellular view of E1 docked in the open state model of $I_{Ks}$ from Kang *et al.* I145 in S1 and V324 in S6 of Q1 are in yellow space-fill representations. (*C*) Side view of Kang *et al.* open model.

There was considerably less cross-linking of the E1-TM flank to the flanks of S2–S5. Of the 16 combinations of a Cys in the S3-S4 loop and a Cys in the flank of the E1-TM, only one pair, Q1 Q220C and E1 E43C, was significantly (38%) cross-linked (Fig. 2*B*). One Cys, A149C, furthest from the membrane in the S2 flank, and G40C, furthest from the membrane in the E1 flank, were ≈30% cross-linked. Most other pairs in E1 and in S2–S5 were considerably <20% cross-linked.

We take the extent of cross-linking as a reflection of the relative proximity of the substituted Cys (25). Given the predicted three-dimensional arrangement of the TM helices of Q1 (28), we place the extracellular end of E1-TM in a position between the extracellular flanks of S1 and S6 of neighboring Q1 subunits, with diametrically opposite voltage-sensor domains (Fig. 3*A*). In this position, the flank of the E1-TM also has access to the S3-S4 linker in a third Q1 subunit (Fig. 3*A*).

**Function of pWT Q1 Coexpressed with WT E1.** The function of pWT Q1 was compared with that of wild-type (WT) Q1, each coexpressed with WT E1. Because the $K^+$ current continued to rise slowly after activation, we used the current at 2 s to calculate an isochronal conductance. Plots of normalized conductance versus voltage (G-V curves) and their characteristic $V_{1/2}$ were indistinguishable for pWT and WT (Fig. S1*A* and Table S1). Over a range of voltages, the rate constants for activation ($k_{act}$) were slightly greater, and the rate constants for deactivation ($k_{deact}$) were slightly smaller, for pWT compared with WT Q1 (Fig. S1*B* and *C* and Table S1). Treatment of the cells with 10 mM DTT had slight effects on pWT function; $k_{deact}$ was slightly smaller and $k_{act}$ was slightly greater at all voltages (Fig. S1*B* and *C* and Table S1).

**Single Cys Mutants.** We focused on four double-Cys mutants that were among the most extensively cross-linked Cys pairs to determine the functional effects of cross-linking the E1-TM flank to S1 or S6. The functional characteristics of the four single Cys mutants, corresponding to these four double-Cys mutants, were at most slightly different from those of pWT. Compared with the channel formed by pWT Q1 and WT E1, $V_{1/2}$ of Q1 I145C and E1 WT, of Q1 V324C and E1 WT, of Q1 WT and E1 K41C, and of Q1 WT and E1 L42C differed by −15 mV, 17 mV, 1 mV, and 15 mV, respectively (Fig. S2 and Table S1). For the same single mutants, $k_{act}{}^{mut}/k_{act}{}^{pWT}$ was 1.2, 0.6, 0.9, and 0.6, and $k_{deact}{}^{mut}/k_{deact}{}^{pWT}$ was 0.6, 0.9, 1.1, and 1.2, respectively. These changes in kinetic constants were small. Thus, none of the native residues are functionally irreplaceable.

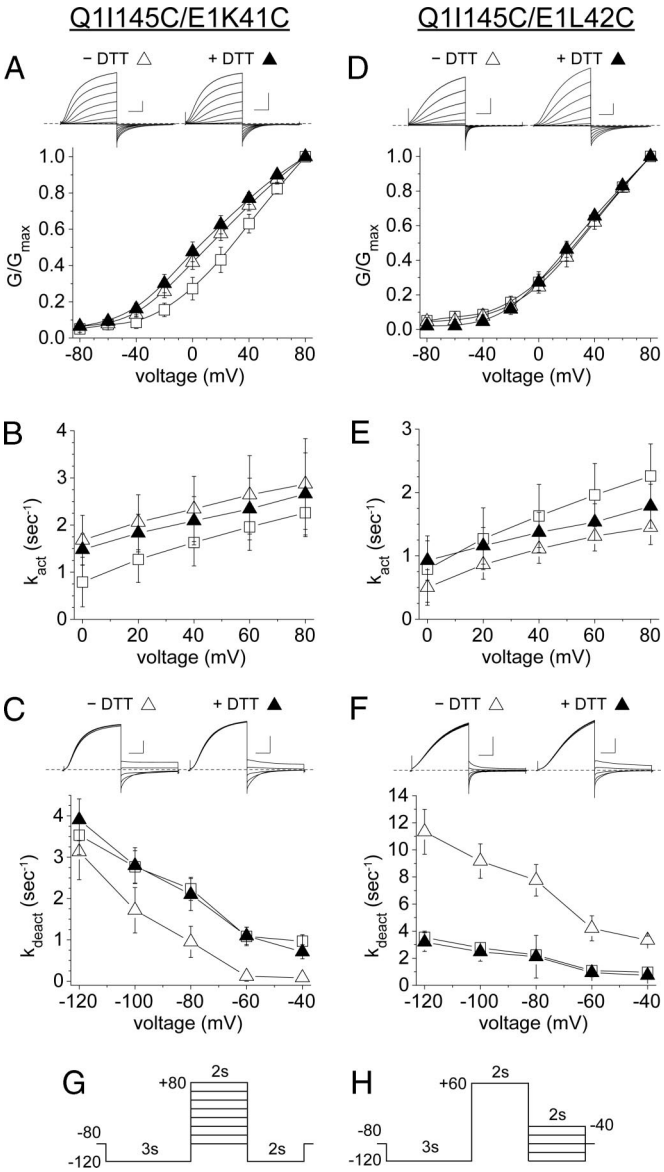


**Fig. 4.** Functional consequences of cross-linking the extracellular flanks of Q1 S1 and E1-TM. (*A*) Dependence $G/G_{max}$, measured at 2 s, on voltage, and (*B*) rate constants of activation ($k_{act}$) for pWT (open squares), Q1 I145C/E1 K41C ($n = 5$, open triangles), and Q1 I145C/E1 K41C + DTT ($n = 5$, closed triangles). (*C*) Rate constants of deactivation ($k_{deact}$) for pWT, Q1 I145C/E1 K41C ($n = 6$), and Q1 I145C/E1 K41C + DTT ($n = 6$). For current traces of Q1 I145C/E1 K41C, vertical scale is 200 pA/pF and horizontal scale is 0.5 s. (*D*) Dependence of $G/G_{max}$ on voltage, taken at 2 s, and (*E*) rate constants of activation ($k_{act}$) for pWT (open squares), Q1 I145C/E1 L42C ($n = 7$, open triangles), and Q1 I145C/E1 L42C + DTT ($n = 4$, closed triangles). (*F*) Rate constants of deactivation ($k_{deact}$) for pWT, Q1 I145C/E1 L42C ($n = 6$), and Q1 I145C/E1 L42C + DTT ($n = 6$). (*G*) Voltage protocol for activation kinetics. (*H*) Voltage protocol for deactivation kinetics. For current traces of Q1 I145C/E1 L42C, vertical scale is 100 pA/pF and horizontal scale is 0.5 s. Dotted lines indicate zero current.

**Functional Effects of Cross-Links Between the Flanks of Q1 S1 and E1-TM.** The major functional perturbation of channels formed from Q1 I145C and E1 K41C was the $k_{deact}$ was much decreased compared with pWT Q1-E1 (Fig. 4*C*), for example, by a factor of 30 at −40 mV (Table S1). This effect was reversed by DTT and, therefore, was due to the disulfide cross-link, *per se* (Fig.

BIOCHEMISTRY

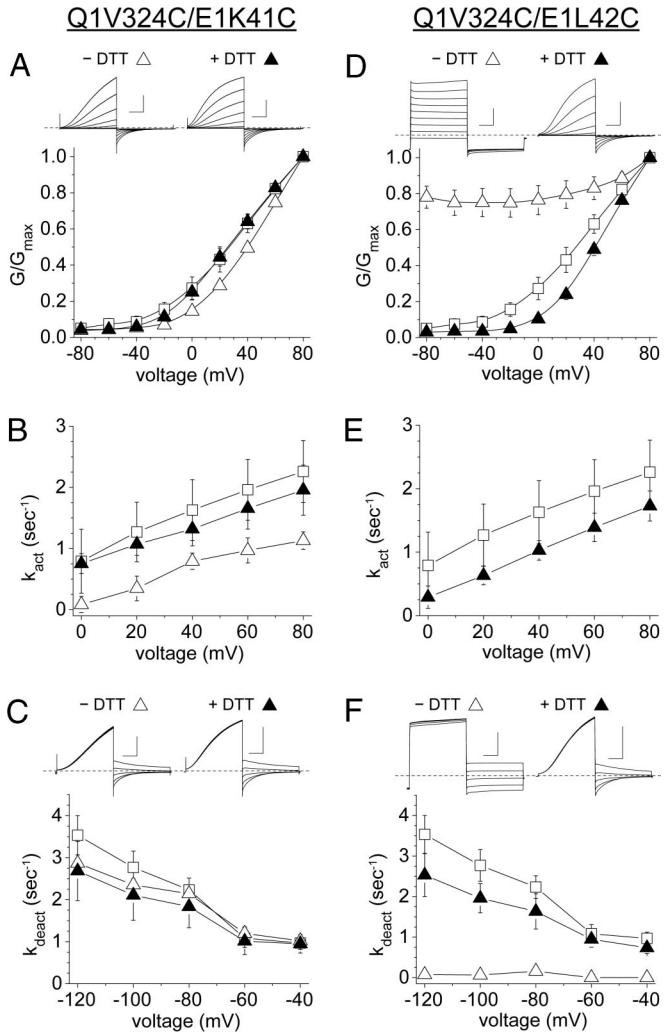


**Fig. 5.** Functional consequences of cross-linking the flanks of Q1 S6 and E1-TM. (*A*) Dependence of $G/G_{max}$ on voltage, taken at 2 s, and (*B*) rate constants of activation ($k_{act}$) for pWT (open squares), Q1 V324C/E1 K41C ($n$ = 5, open triangles), and Q1 V324C/E1 K41C + DTT ($n$ = 4, closed triangles). (*C*) Rate constants of deactivation ($k_{deact}$) for pWT, Q1 V324C/E1 K41C ($n$ = 6), and Q1 V324C/E1 K41C + DTT ($n$ = 6). (*D*) Dependence of $G/G_{max}$ on voltage, taken at 2 s, and (*E*) $k_{act}$ for pWT (open squares), Q1 V324C/E1 L42C ($n$ = 4, open triangles), and Q1 V324C/E1 L42C + DTT ($n$ = 4, closed triangles). (*F*) $k_{deact}$ for pWT, Q1 V324C/E1 L42C ($n$ = 3), and Q1 V324C/E1 L42C + DTT ($n$ = 5). For current traces, vertical scale is 200 pA/pF and horizontal scale is 0.5 s.

4*C*). Moreover, neither single Cys mutation had this effect. The other differences from pWT, a decrease in $V_{1/2}$ by 15 mV and a 30% increase in $k_{act}$, were not reversed by DTT, and the single mutation, Q1 I145C, expressed with WT E1 had the same effect (Fig. 4*A* and Table S1).

The cross-link between the Q1 I145C to the next residue in the E1-TM flank, L42C, also altered $k_{deact}$, but in the opposite direction: $k_{deact}$ was increased at all voltages tested (3-fold at −40 mV), and this effect was completely reversed by DTT (Fig. 4*F* and Table S1). The G-V curve of the double mutant was not different from pWT, either before or after treatment with DTT (Fig. 4*D*), and $k_{act}$ was slightly decreased (Fig. 4*E*).

**Functional Effects of Cross-Links Between the Flanks of Q1 S6 and E1-TM.** The pair Q1 V324C and E1 L42C, which was approximately 70% cross-linked (Fig. 2*B*), yielded constitutively open channels (Fig. 5*D*). This cross-linked species was open at all tested voltages, although there was a suggestion that a small population of channels could close at −120 mV (Fig. 5 *D* and *F*). Because the current was ohmic, activation kinetics could not be obtained. Deactivation was very slow or nonexistent. This effect was due to the disulfide bond because after incubation in 10 mM DTT, the G-V curve and kinetics of the reduced Cys pair were similar to those of pWT (Fig. 5 *D–F* and Table S1).

The disulfide from Q1 V324C to E1 K41C had different and modest effects: the largest was that $k_{act}$ was less at all voltages (60% at + 60 mV) (Fig. 4*B*). Also, the G-V curve was slightly right-shifted (Fig. 5*A*). Both effects were reversed by DTT. $k_{deact}$ was unaltered (Fig. 5*C*).

After DTT treatment of Q1 V324C - E1 L42C, which restored pWT-like function, removal of the DTT resulted in a partial restoration of the constitutively open state. This spontaneous reformation of the disulfide occurred at the same rate in the open and closed states, at least at the resolution (5 s) of our measurements (Fig. S3 *D–G*). The restoration of the constitutively open state was blocked by washing out the DTT with 2 mM N-ethylmaleimide, thereby rapidly alkylating all free Cys thiols (Fig. S3*G*). Equivalent state-dependence experiments were carried out on pWT channels with no indication of functional change during DTT wash-out (Fig. S3 *A–C*).

## Discussion

**Location of E1.** The disulfide cross-linking that we measured was restricted to channels transported to the cell surface. Because the cell selects against transporting misfolded or misassembled proteins (32, 33), the structures of these channels are likely to be at least near native. Also, to the extent that disulfide formation was catalyzed by protein disulfide isomerase homologs in the endoplasmic reticulum (34), the greater the extent of cross-linking, the closer on average the two Cys were in a relatively stable conformation of the channel before cross-linking (25). If the disulfides were formed by spontaneous oxidation, the rate of such formation, and hence the extent of formation, also increases with the proximity of the two Cys, notwithstanding that thermal motion can result in relatively slow disulfide bond formation between distant sulfhydryls (35, 36).

We determined the extents of disulfide formation between Cys substituted in the extracellular flank of E1-TM and Cys substituted in the flanks of S1 through S6 of Q1. We found >40% cross-linking between the E1-TM flank and the S1 flank in 10 Cys pairs and between the E1 flank and the S6 flank in 3 Cys pairs (Fig. 2). Between E1 and the S3-S4 linker, only E1 E43C and Q1 Q220C were significantly cross-linked. There were lower extents of cross-linking from E1 to S2 and even less to S5.

Assuming the similarity of the structures of the Q1 tetramer and the known structures of other voltage-gated $K^+$channels, we infer from our cross-linking results that the E1-TM docks between S1 and S6 from two Q1 subunits (Fig. 3*A*). We placed the E1-TM in a theoretical model of Q1 (28), based on the crystal structure of Kv1.2 in the open state (27). Our placement is consistent with a recent structural model of the E1-Q1 complex (37) (Fig. 3 *B* and *C*). Our preliminary results (38) were cited in support of this model, in which both I145 in S1 and V324 in S6 are oriented toward E1. This model, however, does not include the flanking region of E1-TM.

The pattern of disulfide bond formation is consistent with relatively free rotation of the S1 flank, but not the S6 flank, and flexibility of the E1 flank (Fig. 2 *C* and *Results*).

Previous work by others examined the interactions of E1 with a subset of the Q1 TM helices. There is much evidence that the E1-TM is close to S6 (15–17). Tapper and George (15) found that $Cd^{2+}$ intercalated between S6 C331 and E1 F54C and G55C.

Xu *et al.* (23) recently reported cross-linking between one Cys substituted in the Q1 S1 flank, I145C, and G40C or K41C in the E1-TM flank and hypothesized that E1 resides between S1, S6,

and S4 of three different Q1 subunits. Nakajo and Kubo (18) observed cross-linking between E44C in rat E1 (aligns with E43 in human E1 used here) and A226C in S4 of Q1, which is ≈5 residues into the membrane (Fig. 1*A*). Our observation that E1 E43C cross-linked to Q1 Q220C is consistent with E1-TM interacting with S4 (Fig. 2*B*). More recently, Shamgar *et al.* (39) also suggested that E1 might lie between S1 and S4 of two different Q1 subunits.

**Functional Consequences of Cross-Linking.** We tested four of the most readily cross-linked double Cys mutants for function. All of these channels opened; not all closed. Most dramatically, the cross-link between Q1 V324C and E1 L42C resulted in a constitutively open channel, in which deactivation was very slow even at extremely hyperpolarized voltages; i.e., the open state was stabilized. Cross-linking from the same Q1 position, V324C, to E1 K41C, adjacent to L42C, had opposite, though small effects: These were a speeding of deactivation, a slowing of activation, and an increase in $V_{1/2}$; i.e., a slight stabilization of the closed state. Cross-linking of E1 K41C to Q1 I145C and E1 L42C to Q1 I145C also had opposing effects: Cross-linking 41 to 145 slowed deactivation 30-fold at −40 mV, while cross-linking 42 to 145 speeded deactivation 3-fold. The corresponding effects on activation were modest but nonetheless favoring the open state in 41–145 and the closed state in 42–145.

For the Q1 I145C-E1 G40C pair, Xu *et al.* (23) observed that a disulfide cross-link suppresses deactivation. Contrary to our finding that the cross-link from E1 K41C to S1 I145C also slowed deactivation, Xu *et al.* (23) found that this cross-link stabilized the closed state. The different observations could be due to the different pseudowild-type Q1s used by Xu *et al.* (23) and us. Nevertheless, approximately oppositely orientated cross-links from E1 resulted in approximately opposite functional effects.

It is axiomatic that the modulation by E1 of the function of Q1 involves differences in their physical interaction in different states of the channel. Xu *et al.* (23) proposed that "wobble" of E1 between S1 and S4 might contribute to the unique slow activation of $I_{KS}$. Restier *et al.* (40) proposed that E1 might slow activation by altering the making and breaking of salt bridges between S2 and S4, presumably through an indirect interaction with S1 within the same voltage-sensor bundle. Additionally, they investigated the effects of the gain-of-function atrial fibrillation associated mutations in S1, S140G and V141M, and proposed that these mutations might exert their effect through altered docking between S1 and E1, which, in turn, alters interactions between E1 and S5 and S6. Implicit in their proposal is that E1 might couple the voltage sensor and the pore. Kang *et al.* (37) proposed that an adhesive interface between Q1 and E1 in the closed state must be overcome in the transition to the open state and that this results in the slow activation of $I_{KS}$.

As stated above, the patterns of disulfide cross-linking from the E1-TM flank to the S1 and S6 flanks (Fig. 2*C*) suggest that the E1 extracellular flank, at least, is flexible. Notwithstanding, cross-linking this flank in approximately opposite directions could impose a torque on E1-TM, shifting the free energy of interaction of E1-TM with S1, S6, and S4, and thereby the free-energy differences among the open state, the closed state, and the connecting transition states. Consistent with our cross-linking results and the work of others, we suggest in the absence of cross-linking, the axial rotation of E1-TM is different in the open and closed state of the channel, a manifestation of the different interactions between E1-TM and the Q1 TM helices in the open and closed states. This would be a mechanism whereby the structural changes in the membrane domain are transmitted to E1-Q1 interactions in the cytoplasmic domain.

## Materials and Methods

**Molecular Biology and Cell Culture.** Human E1 (41) was subcloned into the p3XFLAG-CMV-14 Expression Vector (Sigma E4901) to generate a C-terminal FLAG-tagged E1. Mutations were engineered into human Q1 (10) and E1 cDNA with the QuikChange Site-Directed mutagenesis kit (Stratagene). All biochemical experiments were conducted with these constructs. Human E1 with an N-terminal HA tag was used for functional studies. Chinese hamster ovary (CHO) cells (American Type Culture Collection) were cultured in Ham's F-12 culture media with 10% fetal bovine serum in a 37°C incubator with 5% $CO_2$.

**Electrophysiology.** Currents were recorded at room temperature using the whole-cell patch clamp configuration with an Axopatch 200A amplifier (Axon Instruments) as previously described (12). Test solutions were applied by local perfusion, which allowed relatively rapid (< 0.5 sec) (42) changes of experimental solutions near the cell. Series resistance was 3–8 MΩ. CHO cells were cotransfected with Q1 C214A-C331A (pWT Q1) or Cys-substituted mutants in the pWT background, with WT E1 or Cys-substituted mutants of E1, and with eGFP (0.4 μg of each construct) and plated on small Petri dishes. Electrophysiological measurements were carried out 48 h after transfection. The external solution was pH 8.0 to facilitate reduction by DTT and contained (in mM): NaCl 132, KCl 4.8, $MgCl_2$ 1.2, $CaCl_2$ 1, glucose 5, Hepes 10, and, when called for, DTT 10. Internal solution was pH 7.3 and contained: $K^+$ aspartate 110, $MgCl_2$ 1, $CaCl_2$ 1, EGTA 11, $K_2ATP$ 5, and Hepes 10. Cells were chosen based on eGFP fluorescence. Data were collected using pClamp v. 8.0 and analyzed as described previously (12) with Origin (Microcal).

Cells were held at −80 mV. For activation, cells were prepulsed to −120 mV for 3 s, depolarized from −80 to +80 mV in increments of 20 mV for 2 s, followed by a repolarization at −120 mV for 2 s. For deactivation, cells were prepulsed to −120 mV, depolarized to + 60 mV, followed by repolarizations from −40 mV to −120 mV in 20 mV increments. For the single pulse protocol in Fig. 5*D*, cells were depolarized to +60 mV for 2 s followed by repolarization at −40 mV for 2 s, repeated once every 15 s.

To determine $k_{act}$, data from the activating phase of the activation protocols were reduced to one sample per 10 ms by averaging, baseline subtracted, then fit with the equation $i = i_{max}*[1 - \exp(-k_{act}*t)]^n$ in SigmaPlot 9.0 (SYSTAT) where $i_{max}$, $k_{act}$, and n were allowed to vary. To determine $k_{deact}$, the repolarization phase from the deactivation protocols were reduced to one sample per 10 ms, leak adjusted, then fit with the equation $i = y_0 + A*\exp(-k_{deact}*t)$ where $y_0$, A, and $k_{deact}$ were allowed to vary.

**Cross-Linking.** CHO cells were cotransfected with mutant cDNAs of Q1 and FLAG-E1 (0.4 μg each) using PLUS reagent and Lipofectamine (Invitrogen). Cells were incubated for 48 h at 37°C in the presence of 5% $CO_2$. No cross-linking agents were added. The adherent cells were surface-biotinylated with EZ-Link Sulfo-NHS-LC-Biotin (Pierce), the reaction was stopped, the cells were lysed, and, after sedimentation of insoluble material, the supernatant was mixed with Ultralink Immobilized NeutrAvidin Protein Plus beads (Pierce) to bind the biotin-labeled membrane proteins, which were eluted from the beads by treatment for 3 min at 90°C in 8 M Urea, 4% SDS, 200 mM Tris pH 8.0, and 2 mM EDTA, all as previously described (25). DTT to a final concentration of 19 mM was added to half of each eluate. Samples were incubated at 50°C for 20 min, bromophenol blue was added, and the samples in SDS sample buffer were electrophoresed on 4–20% acrylamide gels. The gels were transferred to nitrocellulose, and the blot was blocked and incubated with goat anti-Q1 antibody (1:1,000, C-20, Santa Cruz) and mouse anti-FLAG antibody (Sigma, M2). Membranes were washed and incubated with donkey anti-goat AlexaFluor 680-labeled antibody (1:5,000, Molecular Probes) and donkey anti-mouse IRDye 800-labeled antibody (1:5,000, Licor). Fluorescent signals were detected using the Odyssey Infrared Imager (Licor).

The extent of cross-linking was calculated based on the intensities of four bands (Fig. S4): the monomeric Q1 band, the cross-linked Q1-E1 band, the $Q1_2$ band, and a band labeled X. The apparent molecular weight of X was >250 kDa and, based on the relative intensities of the anti-Q1 antibody signal from this band and the anti-FLAG antibody signal, normalized by these same signals from the Q1-E1 band, X contained approximately 2 Q1 per E1. Thus, we calculated the extent of cross-linking of the total Q1 in each lane as $(Q1E1 + X/2)/(Q1 + Q1E1 + Q1_2 + X)$. The inclusion of the two higher molecular weight bands, $Q1_2$ and X, in the calculation resulted in a lower estimate for the extent of cross-linking than that calculated from just Q1 and Q1-E1.

**ACKNOWLEDGMENTS.** We thank Jenny Rao for technical assistance and Jason Baek for IT help. This work was supported in part by National Institutes of Health Grants HL44365 (to R.S.K.), HL68093 (to S.O.M.), HL081172 (to A.K.) and Medical Scientist Training Program GM07367 (to D.Y.C.). J.R.B. is supported by National Institutes of Health Training Grant T32 HL087745.

1. Kass RS, Wiegers SE (1982) The ionic basis of concentration-related effects of noradrenaline on the action potential of calf cardiac purkinje fibres. *J Physiol* 322:541–558.
2. Sanguinetti MC, Jurkiewicz NK (1990) Two components of cardiac delayed rectifier K+ current. Differential sensitivity to block by class III antiarrhythmic agents. *J Gen Physiol* 96:195–215.
3. Wang KW, Goldstein SA (1995) Subunit composition of minK potassium channels. *Neuron* 14:1303–1309.
4. Chen H, Kim LA, Rajan S, Xu S, Goldstein SA (2003) Charybdotoxin binding in the I(Ks) pore demonstrates two MinK subunits in each channel complex. *Neuron* 40:15–23.
5. Morin TJ, Kobertz WR (2008) Counting membrane-embedded KCNE beta-subunits in functioning K+ channel complexes. *Proc Natl Acad Sci USA* 105:1478–1482.
6. Splawski I, *et al.* (2000) Spectrum of mutations in long-QT syndrome genes. KVLQT1, HERG, SCN5A, KCNE1, and KCNE2. *Circulation* 102:1178–1185.
7. Bellocq C, *et al.* (2004) Mutation in the KCNQ1 gene leading to the short QT-interval syndrome. *Circulation* 109:2394–2397.
8. Chen YH, *et al.* (2003) KCNQ1 gain-of-function mutation in familial atrial fibrillation. *Science* 299:251–254.
9. Hong K, *et al.* (2005) De novo KCNQ1 mutation responsible for atrial fibrillation and short QT syndrome in utero. *Cardiovasc Res* 68:433–440.
10. Sanguinetti MC, *et al.* (1996) Coassembly of K(V)LQT1 and minK (IsK) proteins to form cardiac I(Ks) potassium channel. *Nature* 384:80–83.
11. Barhanin J, Lesage F, Guillemare E, Fink M, Lazdunski M, Romey G (1996) K(V)LQT1 and IsK (minK) proteins associate to form the I(Ks) cardiac potassium current. *Nature* 384:78–80.
12. Kurokawa J, Chen L, Kass RS (2003) Requirement of subunit expression for cAMP-mediated regulation of a heart potassium channel. *Proc Natl Acad Sci USA* 100:2122–2127.
13. Chen H, Sesti F, Goldstein SA (2003) Pore- and state-dependent cadmium block of I(Ks) channels formed with MinK-55C and wild-type KCNQ1 subunits. *Biophys J* 84:3679–3689.
14. Kurokawa J, Motoike HK, Kass RS (2001) TEA(+)-sensitive KCNQ1 constructs reveal pore-independent access to KCNE1 in assembled I(Ks) channels. *J Gen Physiol* 117:43–52.
15. Tapper AR, George AL, Jr. (2001) Location and orientation of minK within the I(Ks) potassium channel complex. *J Biol Chem* 276:38249–38254.
16. Melman YF, Um SY, Krumerman A, Kagan A, McDonald TV (2004) KCNE1 binds to the KCNQ1 pore to regulate potassium channel activity. *Neuron* 42:927–937.
17. Panaghie G, Tai KK, Abbott GW (2006) Interaction of KCNE subunits with the KCNQ1 K+ channel pore. *J Physiol* 570:455–467.
18. Nakajo K, Kubo Y (2007) KCNE1 and KCNE3 stabilize and/or slow voltage sensing S4 segment of KCNQ1 channel. *J Gen Physiol* 130:269–281.
19. Takumi T, *et al.* (1991) Alteration of channel activities and gating by mutations of slow ISK potassium channel. *J Biol Chem* 266:22192–22198.
20. Tapper AR, George AL, Jr. (2000) MinK subdomains that mediate modulation of and association with KvLQT1. 116:379–390.
21. Gage SD, Kobertz WR (2004) KCNE3 truncation mutants reveal a bipartite modulation of KCNQ1 K+ channels. *J Gen Physiol* 124:759–771.
22. Chouabe C, *et al.* (2000) Novel mutations in KvLQT1 that affect Iks activation through interactions with Isk. *Cardiovasc Res* 45:971–980.
23. Xu X, Jiang M, Hsu KL, Zhang M, Tseng GN (2008) KCNQ1 and KCNE1 in the IKs channel complex make state-dependent contacts in their extracellular domains. *J Gen Physiol* 131:589–603.
24. Bass RB, Miller AS, Gloor SL, Falke JJ (2007) The PICM chemical scanning method for identifying domain-domain and protein–protein interfaces: Applications to the core signaling complex of E. coli chemotaxis. *Methods Enzymol* 423:3–24.
25. Liu G, *et al.* (2008) Position and Role of the BK Channel {alpha} Subunit S0 Helix Inferred from Disulfide Crosslinking. *J Gen Physiol* 131:537–548.
26. Liu G, *et al.* (2008) Locations of the beta1 transmembrane helices in the BK potassium channel. *Proc Natl Acad Sci USA* 105:10727–10732.
27. Long SB, Campbell EB, Mackinnon R (2005) Crystal structure of a mammalian voltage-dependent Shaker family K+ channel. *Science* 309:897–903.
28. Smith JA, Vanoye CG, George AL, Jr., Meiler J, Sanders CR (2007) Structural models for the KCNQ1 voltage-gated potassium channel. *Biochemistry* 46:14141–14152.
29. Rost B, Casadio R, Fariselli P, Sander C (1995) Transmembrane helices predicted at 95% accuracy. *Protein Sci* 4:521–533.
30. Jiang Y, *et al.* (2003) X-ray structure of a voltage-dependent K+ channel. *Nature* 423:33–41.
31. Chandrasekhar KD, Bas T, Kobertz WR (2006) KCNE1 subunits require coassembly with K+ channels for efficient trafficking and cell surface expression. *J Biol Chem* 281:40015–40023.
32. Nikles D, Tampe R (2007) Targeted degradation of ABC transporters in health and disease. *J Bioenerg Biomembr* 39:489–497.
33. Nakatsukasa K, Brodsky JL (2008) The recognition and retrotranslocation of misfolded proteins from the endoplasmic reticulum. *Traffic* 9:861–870.
34. Wilkinson B, Gilbert HF (2004) Protein disulfide isomerase. *Biochim Biophys Acta* 1699:35–44.
35. Butler SL, Falke JJ (1996) Effects of protein stabilizing agents on thermal backbone motions: A disulfide trapping study. *Biochemistry* 35:10595–10600.
36. Nagy JK, Lau FW, Bowie JU, Sanders CR (2000) Mapping the oligomeric interface of diacylglycerol kinase by engineered thiol cross-linking: Homologous sites in the transmembrane domain. *Biochemistry* 39:4154–4164.
37. Kang C, *et al.* (2008) Structure of KCNE1 and implications for how it modulates the KCNQ1 potassium channel. *Biochemistry* 47:7999–8006.
38. Chung DY, *et al.* (2008) Cysteine substitution reveals novel inter-subunit interactions in the Iks potassium channel. *Biophys J* 94:82a.
39. Shamgar L, *et al.* (2008) KCNE1 constrains the voltage sensor of Kv7.1 K+ channels. *PLoS ONE* 3:e1943.
40. Restier L, Cheng L, Sanguinetti MC (2008) Mechanisms by which atrial fibrillation-associated mutations in the S1 domain of KCNQ1 slow deactivation of IKs channels. *J Physiol* 586:4179–4191.
41. Murai T, Kazikuza A, Takumi T, Ohkubo H, Nakanishi S (1989) Molecular cloning and sequence analysis of human genomic DNA encoding a novel membrane protein which exhibits a slowly activating potassium channel activity. *Biochem Biophys Res Commun* 161:176–181.
42. Kass RS, Arena JP (1989) Influence of pHo on calcium channel block by amlodipine, a charged dihydropyridine compound: Implications for location of the dihydropyridine receptor. *J Gen Physiol* 93:1109–1127.